

RESEARCH

Open Access



Knockdown of CENPM activates cGAS-STING pathway to inhibit ovarian cancer by promoting pyroptosis

Wei Xie¹, Leiyang Zhang¹, Junjing Shen¹, Fengdi Lai¹, Wenling Han^{1*} and Xiaoyan Liu^{1*}

Abstract

Objective We aimed to screen novel gene signatures for ovarian cancer (OC) and explore the role of biomarkers in OC via regulating pyroptosis using bioinformatics analysis.

Methods Differentially expressed genes (DEGs) of OC were screened from GSE12470 and GSE16709 datasets. Hub genes were determined from protein–protein interaction networks after bioinformatics analysis. The role of Centromeric protein M (CENPM) in OC was assessed by subcutaneous tumor experiment using hematoxylin–eosin and immunohistochemical staining. Tumor metastasis was evaluated by detecting epithelial-mesenchymal transition-related proteins. The proliferation, migration, and invasion were determined using cell counting kit and transwell assay. Enzyme-linked immunosorbent assay was applied to measure inflammatory factors. The mRNA and protein expression were detected using real-time quantitative PCR and western blot.

Results We determined 9 hub genes (KIFC1, PCLAF, CDCA5, KNTC1, MCM3, OIP5, CENPM, KIF15, and ASF1B) with high prediction value for OC. In SKOV3 and A2780 cells, the expression levels of hub genes were significantly up-regulated, compared with normal ovarian cells. CENPM was selected as a key gene. Knockdown of CENPM suppressed proliferation, migration, and invasion of OC cells. Subcutaneous tumor experiment revealed that CENPM knockdown significantly suppressed tumor growth and metastasis. Additionally, pyroptosis was promoted in OC cells and xenograft tumors after CENPM knockdown. Furthermore, CENPM knockdown activated cGAS-STING pathway and the pathway inhibitor reversed the inhibitory effect of CENPM knockdown on viability, migration, and invasion of OC cells.

Conclusion CENPM was a novel biomarker of OC, and knockdown of CENPM inhibited OC progression by promoting pyroptosis and activating cGAS-STING pathway.

Keywords Ovarian cancer, CENPM, Hub gene, Pyroptosis, cGAS-STING pathway

Introduction

Ovarian cancer (OC) is a kind of prevalent female cancer, with a very poor prognosis and high fatality rates [1, 2]. It is frequently identified at an advanced stage which has a dismal five-year survival rate [3]. Additionally, OC has a variety of etiological, histopathological, and biological features, characterized by slow-progressing and aggressive tumor growth [4, 5]. In the advanced stages of OC, cancer cells spread from the ovaries to the pelvis, abdomen, lungs, or multiple secondary sites, which

*Correspondence:

Wenling Han
52068976@qq.com
Xiaoyan Liu
lxy861219@163.com

¹ Department of Obstetrics and Gynecology, First Affiliated Hospital of Gannan Medical University, No. 23, Qingnian Road, Zhanggong District, Ganzhou City, Jiangxi Province 341000, China



© The Author(s) 2024. **Open Access** This article is licensed under a Creative Commons Attribution 4.0 International License, which permits use, sharing, adaptation, distribution and reproduction in any medium or format, as long as you give appropriate credit to the original author(s) and the source, provide a link to the Creative Commons licence, and indicate if changes were made. The images or other third party material in this article are included in the article's Creative Commons licence, unless indicated otherwise in a credit line to the material. If material is not included in the article's Creative Commons licence and your intended use is not permitted by statutory regulation or exceeds the permitted use, you will need to obtain permission directly from the copyright holder. To view a copy of this licence, visit <http://creativecommons.org/licenses/by/4.0/>. The Creative Commons Public Domain Dedication waiver (<http://creativecommons.org/publicdomain/zero/1.0/>) applies to the data made available in this article, unless otherwise stated in a credit line to the data.

severely limits the efficacy of treatment options that cause fatal clinical outcomes [6]. Currently, platinum-based chemotherapy is the mainstream treatment for OC [7]. Although improved surgical techniques and intensive chemotherapy regimens have improved survival in patients with advanced OC over the past two decades, treatment with non-selective cytotoxic drugs often results in severe toxic effects and transient antitumor responses [8]. Additionally, neurotoxicity, neuropathy, and cardiomyopathy caused by chemotherapy are common side effects that affect the normal life of OC patients [9]. Thus, novel treatment targets of OC are urgent to explore.

Centromeric protein M (CENPM) is a member of centromere proteins [10]. Defects in centromere function can lead to loss or destruction of genomic information, resulting in serious and harmful developmental defects or diseases [11]. The most distinctive feature of malignant tumor cells is their ability to continuously divide and proliferate without control, which may be the result of genomic instability caused by chromosomal instability [12]. CENPM promotes cell cycle progression and inhibits apoptosis by regulating P53 signaling pathway [13]. CENPM has been reported in various cancers. In stomach adenocarcinoma, high expression of CENPM can be used as a novel biomarker for stomach adenocarcinoma, and silencing CENPM inhibits gastric adenocarcinoma cell proliferation through cell cycle protein E1 [14]. CENPM is up-regulated in gastric cancer, which can predict poor prognosis and promote tumor cell proliferation and migration [15]. Knockdown of CENPM exerts a driving effect on the progression of hepatocellular carcinoma and is related to poor clinical features [16]. In addition, centromere proteins like CENPA, CENPB, and CENPC have been widely reported in OC [17, 18]. However, the role of CENPM in OC has not been thoroughly investigated.

Pyroptosis is a process of gasdermin (GSDM)-mediated programmed cell death caused by microbial infection, accompanied by activation of inflammatory bodies and release of the pro-inflammatory cytokines [19, 20]. Pyroptosis is associated with the progression of various diseases, especially malignant tumors [21]. Tumors and pyroptosis have a complicated interaction, and the consequences of pyroptosis on cancer vary depending on tissue and genetic background [22]. The role of pyroptosis in OC has been determined. Curaxin CBL0137 induces caspase-3/ GSDME-dependent pyroptosis through the reactive oxygen species /BAX pathway and also has anti-tumor effects on OC cells in vivo [23]. Diethylhexyl phthalate induces pyroptosis through the SLC39A5/NF- κ B/NLRP3 axis in granulosa cells, which leads to ovarian dysfunction [24]. BI 2536 is a potent anti-OC

drug that inhibits proliferation, blocks cell cycle, induces apoptosis and pyroptosis, and leads to the accumulation of CD8+ T cells at the tumor site [25]. However, whether CENPM affects OC progression by regulating pyroptosis of tumor cells needs further study.

The cyclic guanosine monophosphate-adenosine monophosphate synthase (cGAS)/stimulator of interferon genes (STING) pathway is a crucial pathway to activate the innate immune system [26]. The cGAS-STING pathway, a central cytoplasmic double-stranded DNA sensor, is a key pathway by which innate immunity responds to infection, inflammation, and cancer [27, 28]. Currently, the cGAS-STING pathway has received considerable attention due to its holistic and multifaceted role in cancer immune surveillance [29, 30]. The cGAS-STING pathway is involved in activating or inhibiting the anti-tumor immune response, with the intensity and timing of cGAS-STING pathway activation as well as the type and state of the tumor [31–33]. Nevertheless, whether CENPM interferes with the development of OC through the cGAS-STING pathway remains unclear and needs to be further investigated.

In this investigation, we screened differentially expressed genes (DEGs) based on the datasets associated with OC. Based on the protein–protein interaction (PPI) network constructed by DEGs, we screened out the hub genes related to OC. We assessed the accuracy of the hub genes in predicting and diagnosing OC via comprehensive bioinformatics analysis. CENPM was selected as the research target. Subsequently, we demonstrated the functional involvement and potential pathway of CENPM knockdown in OC progression via pyroptosis at the animal and cellular levels. Herein, we will discuss how CENPM affects the occurrence and progression of OC by regulating pyroptosis. These findings aim to establish CENPM as a potential target biomarker of OC, offering novel perspectives on OC development and prospective therapeutic guidelines for the subsequent focused treatment of OC.

Materials and methods

Dataset selection

The gene expression profiles analyzed in this research were retrieved from the Gene Expression Omnibus (GEO) database (<https://www.ncbi.nih.gov/geo/>). We searched “ovarian cancer” in the GEO database. Datasets were selected based on the following criteria: (i) Microarray or high-throughput sequencing profiling of OC samples from humans or model animals, with control samples provided for comparison; (ii) Analytical reports with sufficient sample size; (iii) the samples were grouped and processed; (iv) The original data could be called. Two microarray datasets, GSE12470 (serous OC)

and GSE16709 (serous OC), were selected for subsequent study.

DEGs analysis

GEO2R (www.ncbi.nlm.nih.gov/geo/geo2r) was employed to obtain original data as well as volcano maps and dataset maps. DEGs were screened out according to the screening criteria of $|\log_{2}FC| \geq 1.1$ and $\text{adj. } p \leq 0.05$ (adj. p : p value adjusted by Benjamini–Hochberg multiple test). The top 15 DEGs in each dataset were selected to plot a gene heat map by R language. DEGs Venn diagrams for GSE12470 and GSE16709 were obtained using Draw Venn Diagram tool (<http://bioinformatics.psb.ugent.be/webtools/Venn/>). The common DEGs were screened out for further analysis.

Functional enrichment analysis of DEGs

The Gene ontology (GO) and Kyoto Encyclopedia of Genes and Genomes (KEGG) enrichment analyses of DEGs were conducted using DAVID (<https://david.ncifcrf.gov/>). The most significantly enriched DEGs were selected to display and plot bar charts as well as bubble plots.

PPI network construction and hub gene identification

STRING (<https://www.string-db.org/>) online tool was used to analyze the DEGs to predict interactions between proteins. PPI networks were constructed according to the confidence interaction score (set at 0.4) and visualized using Cytoscape software (www.cytoscape.org/). Key modules were identified from the PPI network using MCODE (Molecular Complex Detection). Cytoscape plugin CytoHubba Version 0.1 was used to calculate the connectivity of each protein node to screen hub genes.

Analysis of key gene

Pathway enrichment analysis for the hub genes was performed using Metascape (<https://metascape.org/gp/index.html#/main/step1>). GO enrichment chord plot was plotted to reveal the relation between the proteins and pathways as well as the change in pathway function. A principal component analysis (PCA) map was drawn using the hub gene expression in the original sample data as a variable to evaluate whether hub genes can distinguish OC from normal controls. R language was employed to draw the ridge plot of hub genes. The diagnostic accuracy of hub genes was evaluated using the receiver operating characteristic (ROC) curve and area under the curve (AUC). The expression profiles of key genes in OC tumors and normal tissues were analyzed by GEPIA (<http://gepia.cancer-pku.cn/>).

Cell culture and treatment

Human OC cells, SKOV3 (iCell-h195; iCell Bioscience Inc, Shanghai, China), A2780 (iCell-h004; iCell Bioscience Inc), and human normal ovarian epithelial cells, IOSE80 (iCell-h112; iCell Bioscience Inc) were cultured in DMEM medium containing 100 U/mL penicillin, 100 $\mu\text{g}/\text{mL}$ streptomycin, and 10% fetal bovine serum, and incubated in a 37 °C, 5% CO₂ humidified incubator (Thermo Scientific, Wilmington, DE, USA).

SKOV3 and A2780 cells were divided into 5 groups: Control (no treatment), si-NC group (transfected with siRNA NC), si-CENPM-1 (transfected with siRNA1), si-CENPM-2 (transfected with siRNA2), and si-CENPM-3 (transfected with siRNA3). The siRNA sequence information was listed in Table S1. The CENPM knockdown in OC cells was conducted by lentivirus vector (GeneChem Biotechnology Co. Ltd Shanghai, China) transfection. Transfection was performed according to the instructions of the Lipofectamine 3000 liposome transfection kit (Invitrogen, Carlsbad, CA, USA). The knockdown efficiency was determined by real-time quantitative PCR detection (RT-qPCR) after 48 h of transfection. After that, the CENPM-knockdown cells were cultured with 10 μM of RU.521 (cGAS inhibitor; MedChemExpress, New Jersey, USA) to explore the role of the cGAS-STING pathway in OC.

Cell viability detection

After transfection, the CCK-8 assay was carried out to detect the proliferation in each group at four time points: 1 d, 2 d, 3 d, and 4 d. Each group of cells was seeded in 96-well plates with cell suspension (1×10^4 cells) and cultured at 37 °C. Then cells were cultured with a maintenance medium (2% FBS + 98% DMEM). Adding 200 $\mu\text{g}/\text{mL}$ of cell suspension to each well, the 96-well plate was incubated in the incubator for 24 h. After removing the culture medium, the cells were washed twice with DPBS. Subsequently, 90 μL of maintenance medium and 10 μL of CCK-8 solution were added to each well. Subsequently, cells were incubated in CCK-8 reagent for 2 h, and the absorbance at 450 nm was then detected under a microplate reader.

Transwell assay

In the cell migration assay, cells (2×10^4) were added into the upper chamber of the transwell insert (Corning Inc, New York, USA) and cultured for 24 h. For the cell invasion assay, the transwell insert was coated with Matrigel (Becton, Dickinson and Company, New Jersey, USA), and cells (2×10^4) were added into the upper chamber. In the lower chamber of the transwell insert, 600 μL of medium containing 15% fetal bovine serum was added,

and the cells were cultured for 24 h in an incubator. Then Matrigel and cells in the upper chamber were wiped away, washed with PBS, fixed with 4% paraformaldehyde at room temperature for 15 min, washed again with PBS, and stained with 0.1% crystal violet at 37°C for 30 min. Photographs were taken to count the number of cells in each field.

Enzyme-linked immunosorbent assay (ELISA)

The concentrations of IL-6, IL-1 β , and TNF- α were detected using ELISA kits (Esebio, Shanghai, China), following the instructions of manufacturer.

Subcutaneous tumor experiment

Female nude mice (BALB/c-nu; 6–8 weeks old; 18–20 g; SiPeiFu, Beijing, China) were acclimated to the experimental scenarios before model construction and then randomly divided into LV-NC group and LV-CENPM group, with 6 mice in each group. Transfected cells were injected subcutaneously into the right back of mice (5×10^6 per mouse). After 7 d, tumor size was measured weekly. The mice were anesthetized by inhaling 1–1.5% isoflurane mixed with oxygen for 4–5 min and subsequently euthanized by cervical dislocation to obtain the xenografts after 4 weeks. The xenografts were immediately weighed after collection.

All the animals were fed freely and housed in a pathogen-free environment. The procedures for care and use of animals were approved by the Ethics Committee of the First Affiliated Hospital of Gannan Medical University and all applicable institutional and governmental rules regulating the ethical use of animals were followed.

Hematoxylin–eosin (HE) and immunohistochemistry staining

The xenograft specimen of mice was fixed in 4% paraformaldehyde. After dehydration and hyalinization, the xenografts were embedded in paraffin to prepare the sections for subsequent experiments. The sections were stained with hematoxylin–eosin reagent (Solarbio, Beijing, China), following the instructions. The stained tissue sections were observed under an optical microscope. For immunohistochemistry staining, the paraffin-embedded sections were dewaxed and rehydrated, and antigenic repair was performed with sodium citrate. Sections were incubated with 3% H₂O₂ at room temperature to quench endogenous peroxidase activity and closed with BSA for 20 min. After adding primary antibody (Anti-Ki67, 1:400, Abcam) samples were incubated overnight at 4 °C and then incubated for 1 h at 37 °C with a secondary antibody (goat anti-rabbit IgG, 1:200, Abcam). The immunohistochemical images were obtained with an optical microscope.

RT-qPCR

Total RNA was extracted using the TRIZOL reagent (Invitrogen). After diluting with RNase-free ultrapure water, the concentration of RNA and the absorbance values at 260 nm and 280 nm were measured using a UV spectrophotometer. Reverse transcription was performed to synthesize cDNA templates in a PCR thermocycler, and BI7500 quantitative PCR instrument (Applied Biosystems, Foster City, CA, USA) was applied to RT-qPCR with the procedures as follows: 95 °C for 10 min for initial denaturation, 95 °C for 10 s for denaturation, 60 °C for 30 s for annealing, and 36 cycles in total. β -actin was selected as an internal reference. The obtained Ct values were analyzed using the $2^{-\Delta\Delta Ct}$ method. Each experiment was repeated three times. The primer sequences could be found in Table S1 (Takara Bio Inc, Otsu, Shiga, Japan).

Western blot

The proteins were extracted and separated by 10% SDS-PAGE. After being transferred onto polyvinylidene fluoride membranes, the membrane was transferred for 2 h at 4 °C and blocked with 5% non-fat milk-TBST, shaking on a room temperature shaker for 2 h. After blocking and washing the polyvinylidene fluoride membrane with washing solution, then the primary antibody was added. The primary antibodies used in this study were as follow: anti-Caspase-1 (1:1000; Abcam, Cambridge, MA, USA); anti-GSDMD (1:1000; Abcam); anti-NLRP3 (1:1000; Abcam); anti-CENPM (1:2000, Abcam) anti-E-cadherin (1:2000, Abcam); anti-N-cadherin (1:2000, Abcam); anti-vimentin (1:2000, Abcam); anti-cGAS (1:1000; Abcam); anti-p-STING (1:1000; Invitrogen); anti-STING (1:1000; Abcam); anti- β -actin (1:2000; Abcam). The membrane was incubated with shaking at 4 °C overnight. Then adding horseradish peroxidase-labeled goat anti-rabbit IgG (1:5000; Abcam), the membrane was incubated at room temperature with shaking for 1 h. Washing the membrane with TBST 3 times, we performed chemiluminescent detection, exposure, and development to analyze the data. The internal reference was β -actin.

Statistical analysis

The data in this study were processed using GraphPad Prism 8.0 statistical software. Quantitative data were presented as mean \pm standard deviation. Comparisons between two groups were performed using t-tests, and comparisons among multiple groups were performed using one-way ANOVA (analysis of variance). Pairwise comparisons after ANOVA were performed using Tukey's multiple comparisons test. $P < 0.05$ suggested a statistically significant difference.

Results

Identification of DEGs

The GSE12470 dataset contained 43 OC tissue samples (8 early-stage tissues and 35 late-stage tissues) and 10 normal samples, while the GSE16709 dataset contained 17 OC tissue samples and 9 normal samples. The gene datasets were standardized and assessed for cross-comparability, suggesting that the selected samples were centered

and the numerical distribution met the standard, indicating high microarray data quality and cross-comparability (Fig. 1A, B). Using GEO2R for analysis, we screened 2908 DEGs from the GSE12470 dataset and 3038 DEGs from the GSE16709 dataset, and clustering analysis was performed to obtain volcano plot of DEGs (Fig. 1C-D). The top 15 up-regulated and down-regulated genes were selected (Tables S2-3). The DEGs heatmaps revealed that

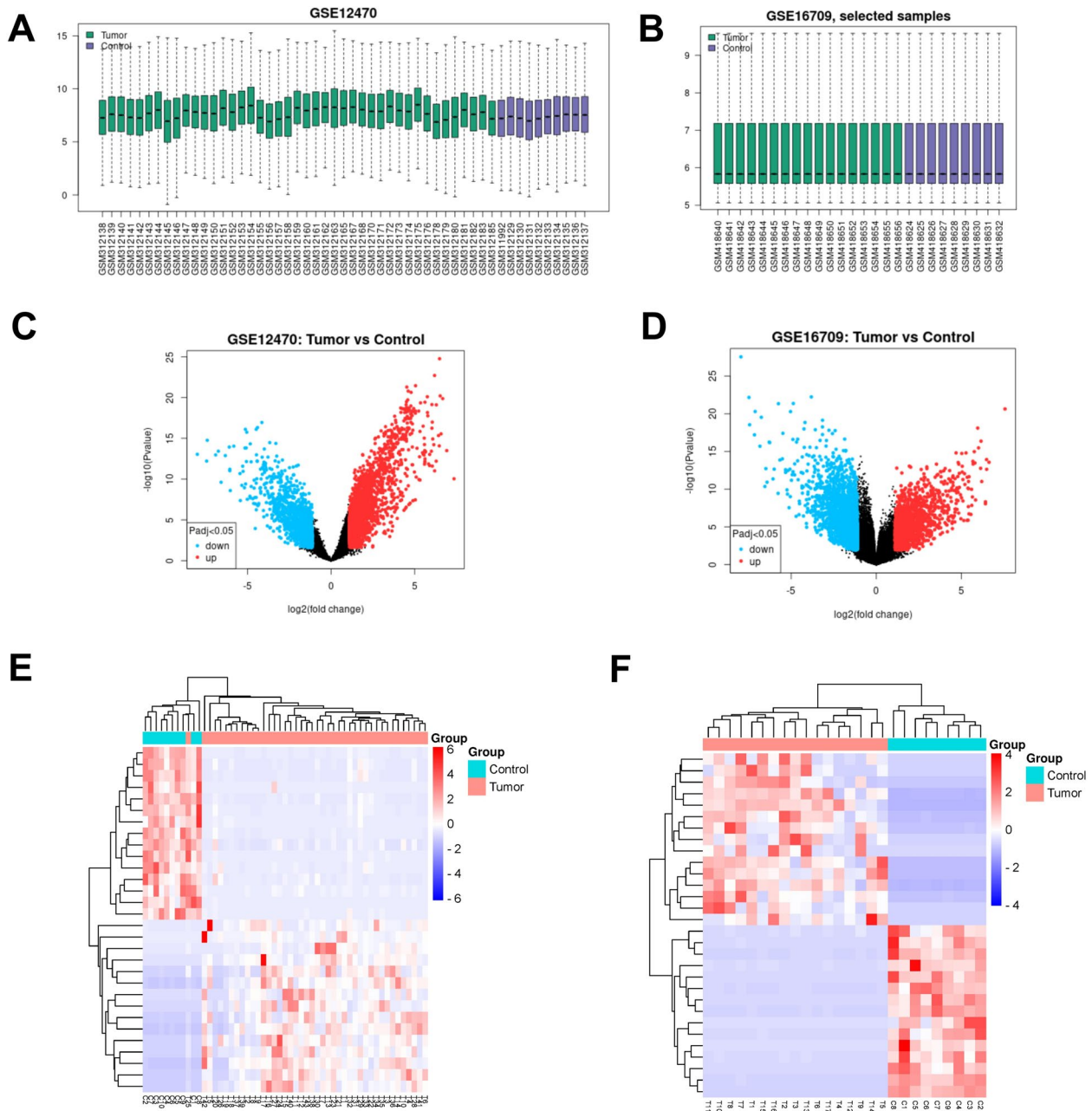


Fig. 1 A-B Cross-comparability evaluation of data set samples; C-D Volcano diagram: The x-coordinate is log₂FoldChange and the y-coordinate is -log₁₀ (p-value). Red dots represent up-regulated genes and blue dots represent down-regulated genes; E Heat map of GSE12470; F Heat map of GSE16709. Horizontal represents genes, and each column is a sample: red for high-expression genes, blue for low-expression genes

the samples were clustered well with high confidence (Fig. 1E-F).

Venn diagrams were drawn to screen the common DEGs between the two datasets (Figure S1), demonstrating that there were 869 DEGs in common between the two datasets.

Function enrichment analysis of common DEGs

The results of the GO enrichment analysis of DEGs were divided into 3 parts: molecular function (MF), biological process (BP), and cellular component (CC). The most significantly enriched top 6 GO terms with the minimum *p*-values of each category were displayed in the histogram and the bubble diagram of GO enrichment analysis (Fig. 2A, Figure S2A). The DEGs were significantly enriched in “extracellular matrix organization,” “cell adhesion,” etc. of BP term; “extracellular matrix organization,” “cell adhesion,” etc. of CC term; and “extracellular matrix organization,” “cell adhesion,” etc. of MF term.

According to the KEGG enrichment analysis results of DEGs, the top 10 pathways with the minimum *p*-value, which means the most significant enriched pathway, were selected for display. The results were shown in the histogram and the bubble diagram of KEGG enrichment analysis (Fig. 2B, Figure S2B). The results revealed that the DEGs were mainly enriched in “Pathways in cancer,” “Focal adhesion,” “ECM-receptor interaction,” “PI3K-Akt signaling pathway,” and “Human papillomavirus infection,” etc.

PPI network construction and hub gene identification

The STRING tool was employed to construct PPI networks based on the DEGs, which were visualized using

Cytoscape software (Figure S3). Key modules were identified from the PPI network of DEGs, and Module 1 with the maximum score was selected (Figure S4). Then, genes in Module 1 were sorted according to the score, and the top 9 genes were selected as hub genes for analysis, including KIFC1, PCLAF, CDCA5, KNTC1, MCM3, OIP5, CENPM, KIF15, and ASF1B.

Analysis of hub genes

GO enrichment chord plot reflected the relationship between proteins and pathways, as well as the changes in the pathway functions (Fig. 3A). After processing with R language, we obtained two principal component variables, PC1 and PC2, which provided a total variance explanation rate of 90.6% and could distinguish between the control group samples and OC samples. The scatter plot suggested that the two groups were separated well, and further confirmed the effectiveness of PC1 and PC2 (Fig. 3B). The ridge line plot showed the expression of hub genes (Fig. 3C).

The ROC curve of hub gene was drawn using the original sample data of GSE12470 and GSE16709 datasets (Figures S5, S6). The results demonstrated that the false positive rate of hub genes (KIFC1, PCLAF, CDCA5, KNTC1, MCM3, OIP5, CENPM, KIF15, and ASF1B) testing in GSE12470 was 0.5%, 0%, 0%, 0%, 0%, 0%, 4.1%, 0%, and 0%, respectively, while the true positive rate was 99.5%, 100%, 100%, 100%, 100%, 100%, 95.9%, 100%, and 100%, respectively. The false positive rate of hub genes in GSE16709 dataset was 3.9%, 2.6%, 15%, 13.7%, 5.6%, 2.6%, 0%, 11.1%, and 13.1%, respectively, while the true positive rate was 96.1%, 97.4%, 85%, 86.3%, 95.4%, 97.4%, 100%, 88.9%, and 86.9%, respectively, indicating that

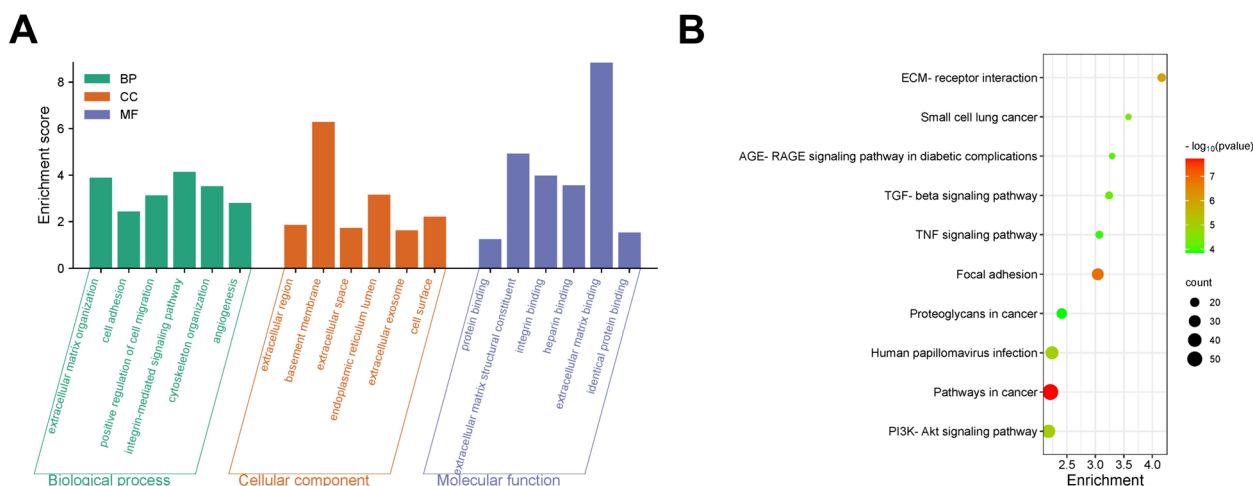


Fig. 2 Analysis of common differentially expressed genes (DEGs) **A** Gene Ontology (GO) enrichment analysis the histogram of DEGs, abscissa is GO term, and ordinate is $-\log_{10}(p\text{-value})$ of enrichment in each term. **B** Bubble map for Kyoto Encyclopedia of Genes and Genomes enrichment analysis

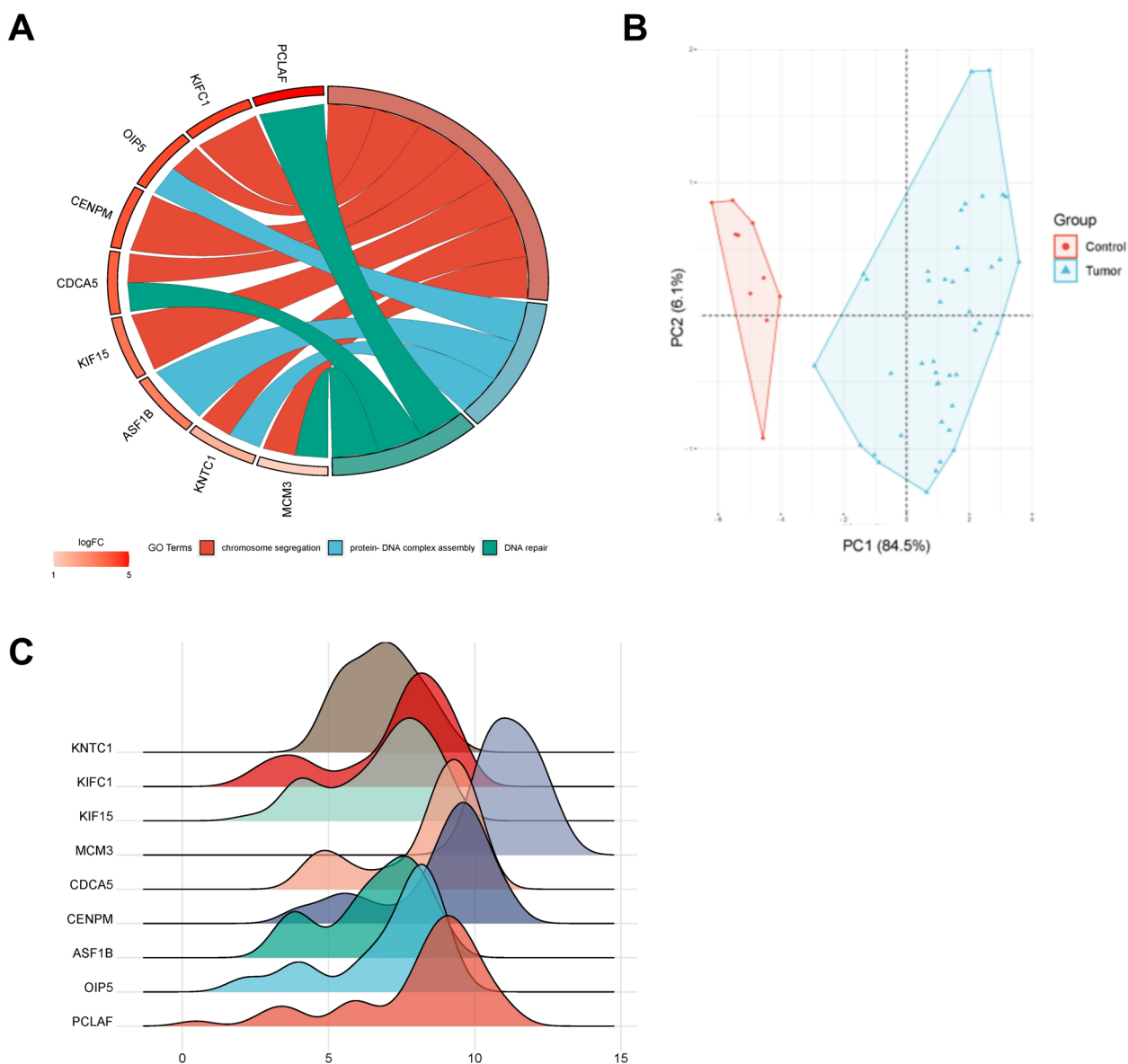


Fig. 3 **A** GO enrichment chord map, the data included 3 parts: genes; logFC is the multiple of gene change, used for sequencing and gene block color; The remaining columns are GO term, and different links of the gene indicate whether the gene is in this GO term; **B** Principal component analysis diagram of hub genes, in which axes PC1 and PC2 are the first and second principal components (i.e., explanation rate of difference by potential variables); Dots represent samples, and different colors represent different groups; **C** Hub gene ridge map, horizontal coordinate is gene expression level, mountain height represents sample abundance of corresponding expression level

hub genes were good indicators to distinguish OC from healthy controls. The differential expression of hub gene in tumor and non-tumor tissues analyzed by The Cancer Genome Atlas database revealed that the expression level of CENPM in tumor tissues was significantly higher than that in normal tissues (Figure S7).

RT-qPCR results suggested that compared to the normal ovarian cells IOSE80, the mRNA expression levels of KIFC1, PCLAF, CDCA5, KNTC1, MCM3, OIP5,

CENPM, KIF15, and ASF1B were significantly up-regulated in SKOV3 and A2780 (Fig. 4).

Knockdown of CENPM suppresses proliferation, migration, and invasion of OC cells

RT-qPCR results revealed that in SKOV3 and A2780 cells, the CENPM expression level in the si-NC group suggested no significant difference, compared with the control group, while the CENPM expression levels

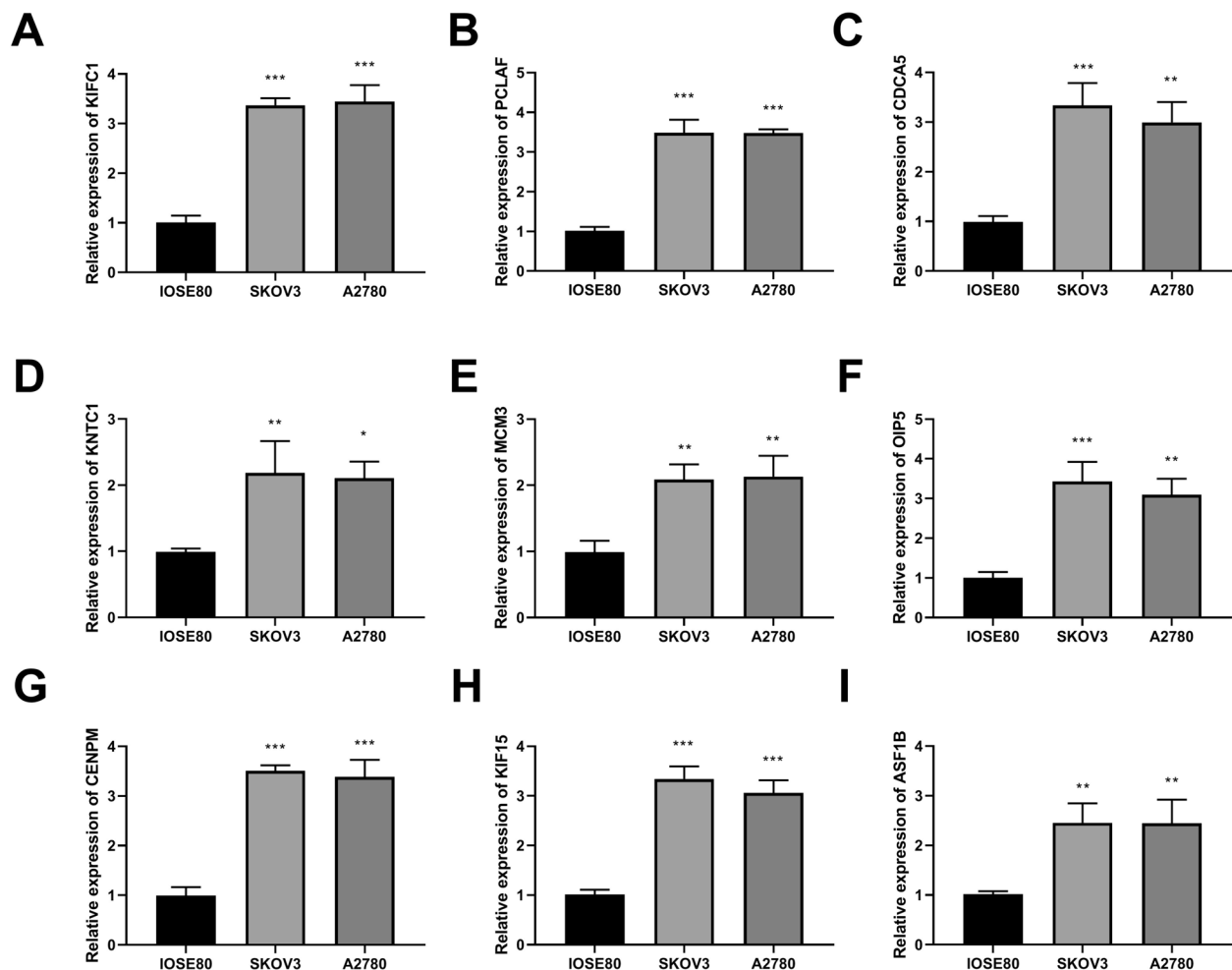


Fig. 4 Real-time quantitative PCR (RT-qPCR) detected the mRNA expression levels of KIFC1, PCLAF, CDCA5, KNTC1, MCM3, OIP5, CENPM, KIF15, and ASF1B in cells. * $P < 0.05$, ** $P < 0.01$, *** $P < 0.001$ vs. IOSE80 cells

in the si-CENPM-1, si-CENPM-2, and si-CENPM-3 groups were significantly decreased (Fig. 5A). Among them, si-CENPM-1 had the highest transfection efficiency. Western blot was performed and showed the same results as RT-qPCR detection, further confirming the RT-qPCR results (Fig. 5B). Therefore, the subsequent experiments were conducted using si-CENPM-1.

CCK-8 results suggested that in SKOV3 and A2780 cells, compared to the control group, there were no significant changes in si-NC group, while cell proliferation of SKOV3 and A2780 cells in the si-CENPM group was significantly suppressed ($P < 0.001$), indicating that knocking down CENPM significantly inhibited the proliferation ability of OC cells (Fig. 5C-D). Additionally, in SKOV3 and A2780 cells, the cell migration, and invasion abilities in the si-CENPM group were notably decreased compared with the control group (Fig. 5E-F).

Knockdown of CENPM promotes pyroptosis in OC cells

Compared to the control group, the concentrations of TNF- α , IL-1 β , and IL-6 in the si-CENPM group were significantly increased (Fig. 6A-B). Western blot assay demonstrated that in SKOV3 and A2780 cells, compared with the control group, the expression levels of pyroptosis-related proteins in the si-CENPM group were significantly increased (Fig. 6C).

Knockdown of CENPM inhibits tumor growth, metastasis, and pyroptosis in mice

The mice in the LV-CENPM group presented significantly lower tumor volumes and weights than those in LV-NC group (Fig. 7A-C). Immunohistochemical staining showed that Ki67 expression level was decreased in LV-CENPM group (Fig. 7D). HE staining suggested that knockdown of CENPM inhibited malignancy of OC (Fig. 7E).

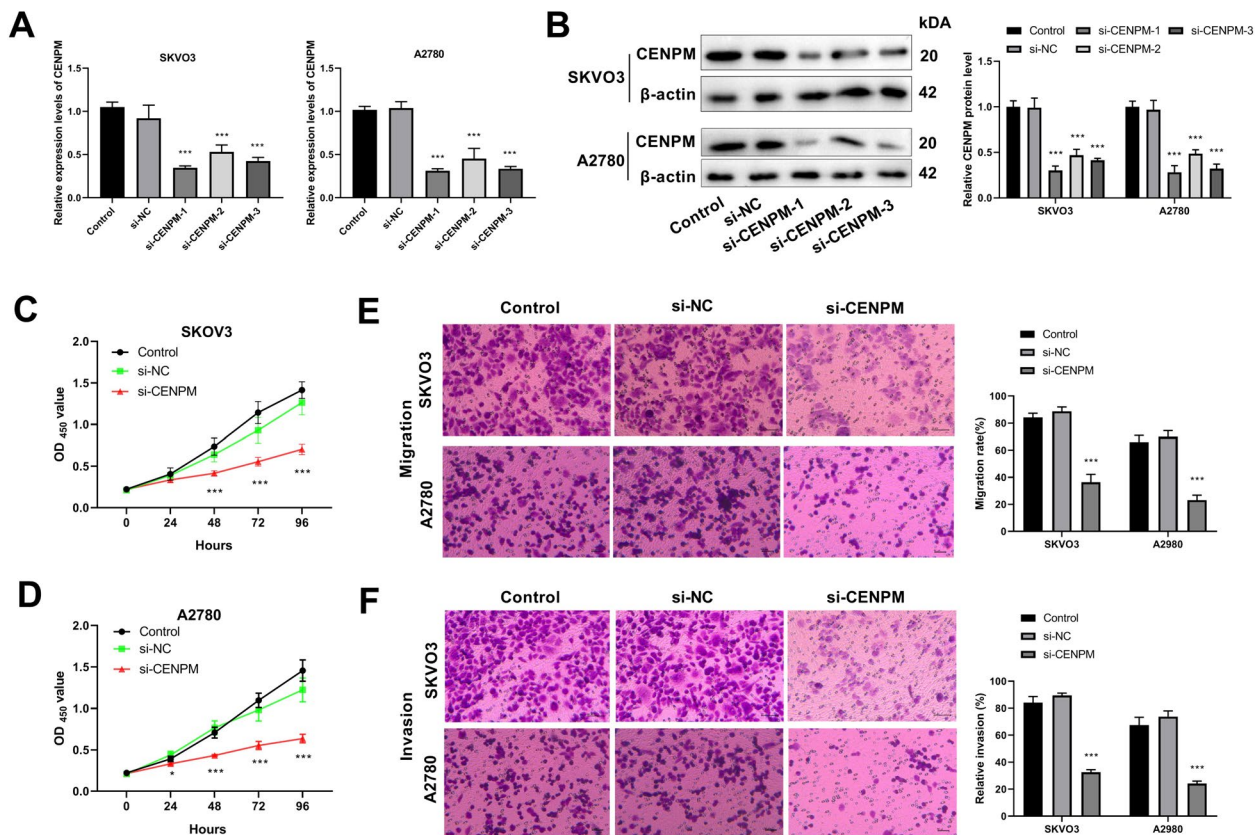


Fig. 5 Effect of CENPM on ovarian cancer cell. **A** RT-qPCR was used to detect transfection efficiency; **B** Western blot was used to detect the protein expression level of CENPM; **C** Cell counting kit was used to detect viability of SKOV3; **D** Cell counting kit was used to detect viability of A2780. **E** Transwell detected cell migration; **F** Transwell assessed the cell invasion. * $P < 0.05$, ** $P < 0.01$, *** $P < 0.001$ vs. Control

Epithelial-mesenchymal transition-related proteins were detected to evaluate tumor metastasis by western blot assay (Fig. 7F). The results showed that knockdown of CENPM increased the protein expression level of E-cadherin, while decreasing the protein expression level of N-cadherin and vimentin. Western blot results demonstrated that the expression level of CENPM protein in tumor tissues of mice was significantly reduced after CENPM knockdown and the expression levels of pyroptosis-related proteins were significantly increased (Fig. 7G). These results further confirmed the inhibitory effect of CENPM knockdown on tumor progression and pyroptosis.

Knockdown of CENPM suppresses the development of OC via activating cGAS-STING pathway

Western blot results revealed that the expression levels of pathway proteins, cGAS, STING, and p-STING in cGAS-STING pathway were significantly higher in si-CENPM group than those in si-NC group (Fig. 8A). Moreover, the treatment of RU.52 reversed the inhibitory effect of

CENPM knockdown on proliferation, migration, and invasion of OC cells (Fig. 8B-D).

Discussion

OC is a heterogeneous disease with the greatest fatality rate and the worst prognosis among gynecological malignancies [34]. Therefore, it is critical to develop new biomarkers for screening in the general population, particularly in high-risk populations such as those with a family history of cancer [35]. Pyroptosis is a non-apoptotic death that has shown great potential in cancer prevention and treatment [36]. In this investigation, we screened and identified the hub genes for OC based on PPI network of DEGs related to OC. The hub genes we selected had highly predictive value for the diagnosis of OC. After literature research, CENPM, a novel gene that has rarely been reported in OC, was screened out as a promising biomarker of OC. CENPM was highly expressed in OC cells. After CENPM knockdown, the migration, invasion, and viability of OC cells, as well as the growth and metastasis of tumors in mice were inhibited, indicating that CENPM silencing

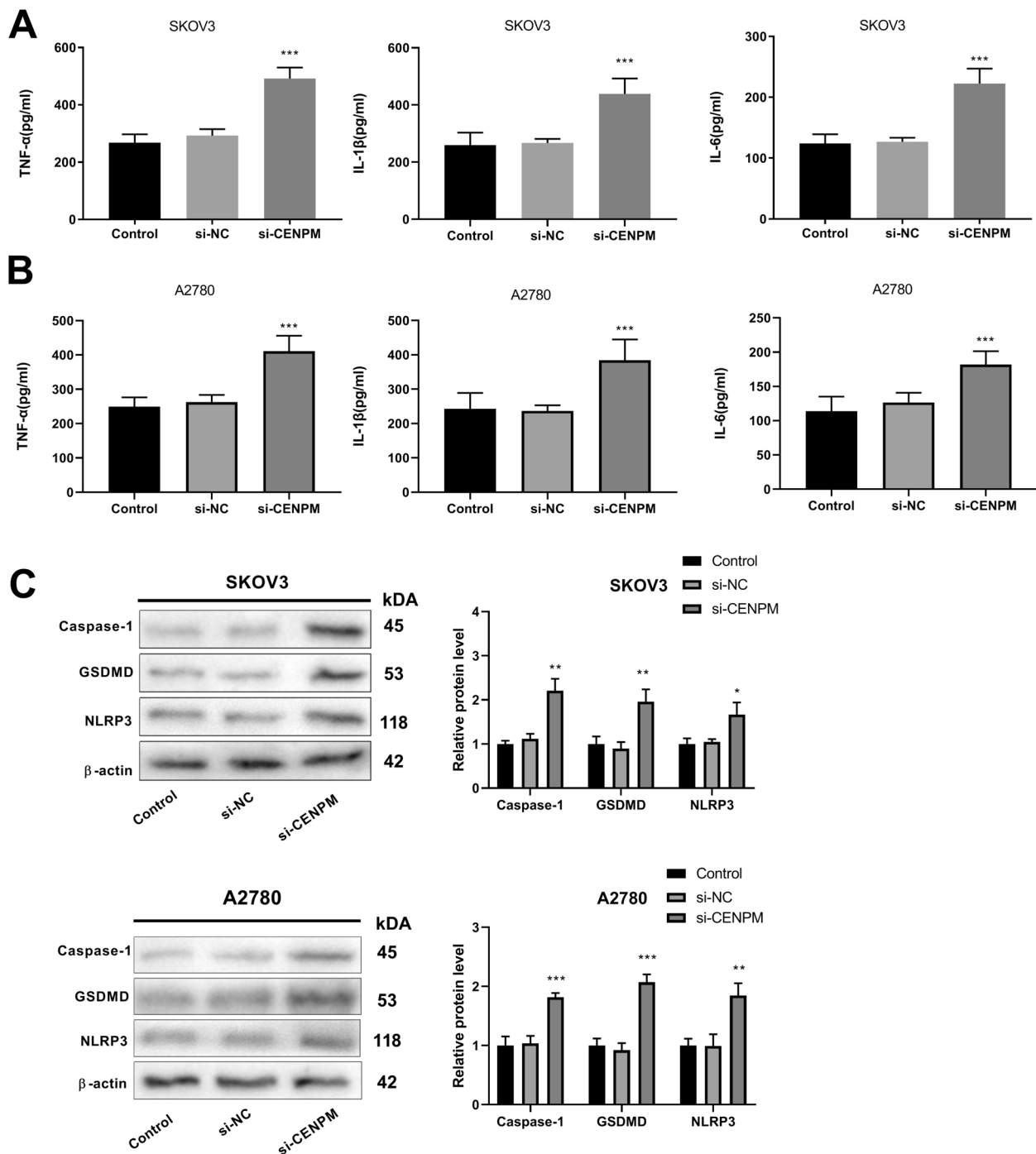


Fig. 6 Effect of CENPM knockdown on pyroptosis. **A** The level of inflammatory factors in SKOV3 cells; **B** The level of inflammatory factors in A2780 cells; **C** Western blot was used to detect the expression of pyroptosis-related proteins in SKOV3 and A2780 cells. * $P < 0.05$, ** $P < 0.01$, *** $P < 0.001$ vs. Control

inhibited the development of OC. We focused on the effect of pyroptosis on OC development. CENPM knockdown promoted pyroptosis in vivo and in vitro. Further study found that knockdown of CENPM activated cGAS-STING pathway and the cGAS-STING

pathway inhibitor reversed the inhibitory effect of CENPM knockdown on OC. Therefore, we concluded that knockdown of CENPM inhibited OC progression by promoting pyroptosis and activating cGAS-STING pathway.

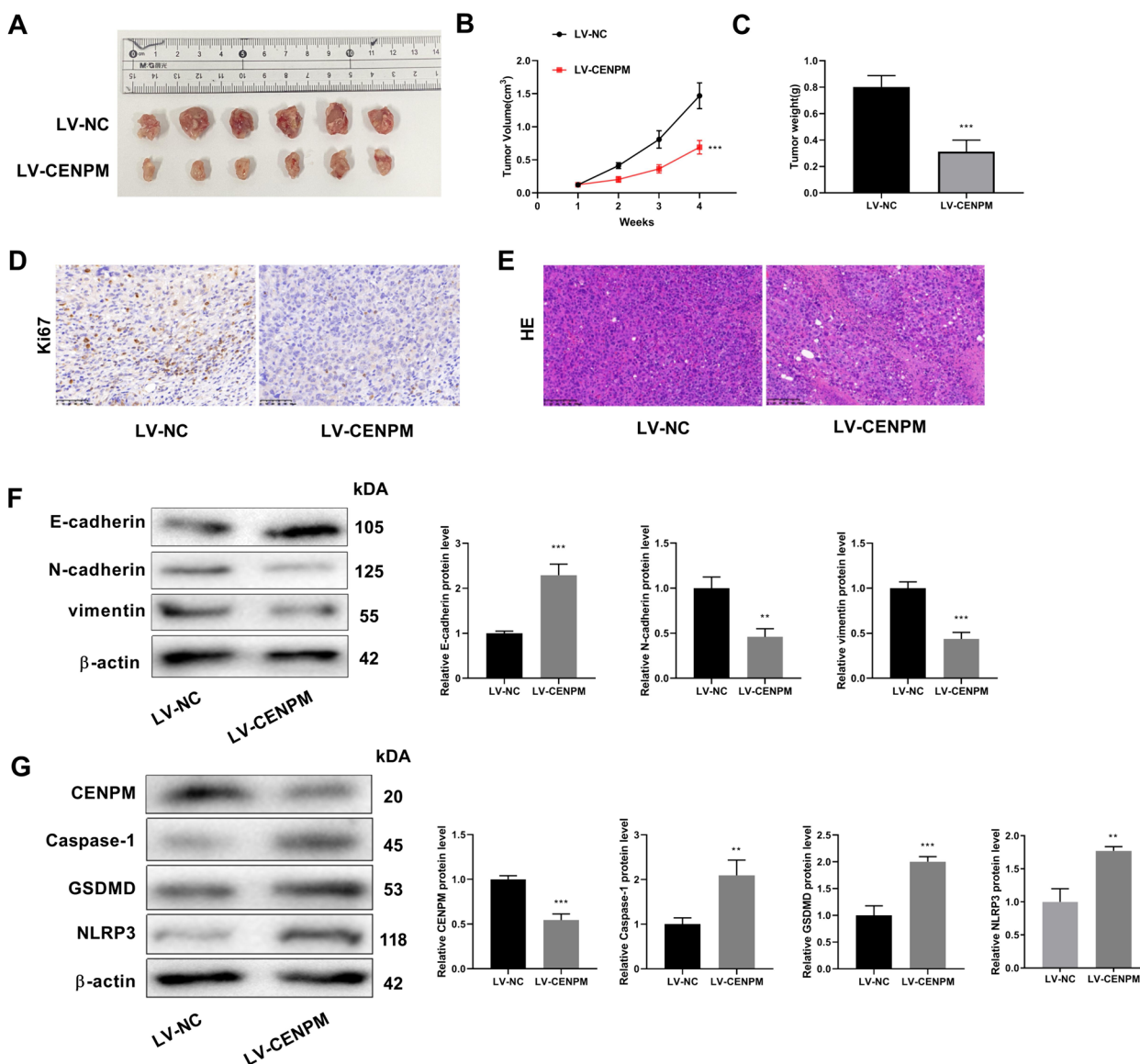


Fig. 7 Effect of CENPM knockdown on tumor. **A** Subcutaneous tumor in each group; **B** Growth curve of subcutaneous tumor in mice; **C** Weight of subcutaneous tumor in mice; **D** Immunohistochemical analysis detected Ki67 levels; **E** Hematoxylin & eosin staining of subcutaneous tumor (Amplification: 200×, Scale: 100 μm); **F** Western blot detected epithelial-mesenchymal transition-related proteins; **G** Western blot to detect the expression of CENPM and pyroptosis-related proteins in tumor tissues. ***P* < 0.01 ****P* < 0.001 vs. LV-NC group

Biomarkers play crucial roles in cancers, and an increasing number of prognostic markers for OC have been identified, making treatment of OC more effective and precise [37]. In this study, we identified KIF1C1, PCLAF, CDCA5, KNTC1, MCM3, OIP5, CENPM, KIF15, and ASF1B as hub genes with high prediction value for OC based on GSE12470 and GSE16709 datasets. KIF1C1 promotes cell proliferation, migration, and epithelial-mesenchymal transition through interaction with CENPE in OC and may be a potential biomarker and therapeutic target for patients with OC [38]. PCLAF

silencing inhibits the proliferation and promotes apoptosis of OC cell lines, which can be used as a target for OC therapy [39]. Based on GSE27651, GSE38666, GSE40595, and GSE66957 datasets, overexpression of CDCA5 in patients with epithelial OC is associated with poor prognosis in patients with epithelial OC, which is one of the hub genes of epithelial OC [40]. Tissue microarray analysis shows that the expression of KNTC1 in vivo is higher in high-grade squamous intraepithelial lesions than in normal cervix, and KNTC1 is a novel tumor suppressor that can prevent the occurrence and development

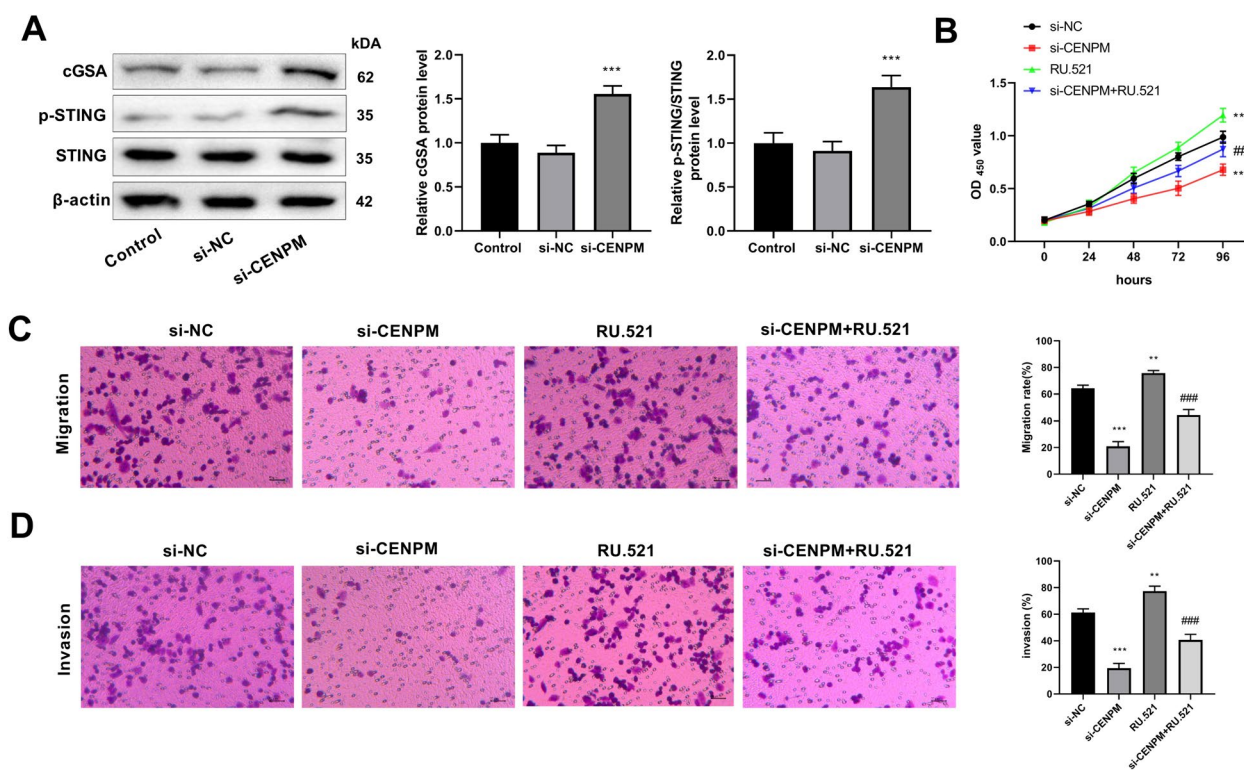


Fig. 8 Effect of CENPM knockdown on cGAS-STING pathway. **A** Western blot was used to detect the protein expression levels of pathway proteins; **B** Cell counting kit was used to detect cell viability. **C** Transwell detected cell migration; **D** Transwell assessed the cell invasion. ** $P < 0.01$, *** $P < 0.001$ vs. Control; ## $p < 0.01$, ### $p < 0.001$ vs. si-CENPM

of cervical cancer [41]. MCM3 is a favorable prognostic marker for salpingo-ovarian high-grade serous carcinoma, and high MCM3 protein levels are also associated with significantly prolonged disease-specific survival [42]. Sangerbox online analysis tool is used to analyze the expression of OIP5 in OC and various human tumors, and OIP5 is highly expressed in OC based on the analysis of GSE12470, GSE14407 and GSE54388 datasets, which may be an important biomarker for the prognosis and diagnosis of OC [43]. By comparative gene expression analysis, CENPM is identified as one of key candidate genes for epithelial OC [44]. Based on the analysis of 91 OC samples and 22 normal ovarian tissues from GSE18520, GSE54388, and GSE27651 gene expression profiles, KIF15 has promising predictive value for the development and prognosis of OC and can be used as a candidate target for the diagnosis and treatment of OC [45]. To construct gene interaction networks based on weighted gene co-expression network analysis, using pancreatic cancer expression profiles from the Cancer Genome Atlas, ASF1B is a promising regulator for pancreatic cancer detection and treatment [46]. All in all, KIF15, PCLAF, CDCA5, KNTC1, MCM3, OIP5, CENPM, KIF15, and ASF1B are hub genes of OC, which

had good specificity and sensitivity in the diagnosis of OC.

Centromere dysfunction, which results in changes in chromosome number, is thought to be closely associated with human cancers [47]. So, as a member of centromeric protein family, CENPM plays a crucial role in progression of various tumors. CENPM is up-regulated in lung adenocarcinoma, which can promote lung adenocarcinoma cell cycle, cell proliferation, migration, and invasion, while inhibiting apoptosis [48]. In pancreatic cancer, CENPM is overexpressed, and down-regulation of CENPM inhibits pancreatic cancer cell proliferation, alters cell cycle, and restricts migration, and invasion [49]. The expression of CENPM is up-regulated in liver cancer, with poor prognosis and silencing CENPM suppresses cell proliferation, migration, and invasion, while depletion of CENPM can promote apoptosis and stagnant cell cycle [13]. We found that CENPM was significantly up-regulated in OC and knockdown of CENPM significantly inhibits proliferation, migration, invasion, and tumor growth of OC. Taken together, knockdown of CENPM suppressed the progression of OC.

Research suggests a link between pyroptosis and OC [50]. Many biomarkers have been implicated in the

pyroptosis of OC cells. A total of 31 DEGs that may affect pyroptosis are screened out between OC and normal ovarian tissue, and 7 of them are identified to be involved in tumor immunity and prognosis prediction of OC, including 3 down-regulated genes (PLCG1, ELANE, PJK) and 4 up-regulated genes (AIM2, CASP3, CASP6, and GSDMA) [51]. The expression of growth-station-specific transcription 5 of lncRNA is inhibited in OC tissues and can cause the development of inflammatory bodies, inducing pyroptosis *in vivo* and *in vitro* [52]. In addition, lncRNA HOTTIP is up-regulated, and its deletion can lead to pyroptosis and hinder the progress of OC [53]. It has been reported that α -Neta directly induces pyroptosis of epithelial OC cells by activating Caspase-4 cleavage of GSDMD, thereby inhibiting their proliferation [54]. In the present study, we illustrated that knockdown of CENPM caused an increase in the expression of pro-inflammatory factors and pyroptosis-related proteins in OC cells and tumors. In brief, knockdown of CENPM promoted pyroptosis to inhibit the development of OC.

Some OC cells suggested unbalanced STING pathway signals by inhibiting STING and its upstream sensor cGAS [55]. Niraparib combined with Entinostat can enhance the cytotoxicity of immune cells by activating the cGAS-STING pathway and promoting the infiltration of pre-immune cells into ascites, thus inhibiting the growth of OC [56]. CX-5461 can make STING transcriptional upregulations mediated by cGAS, thus activating the innate immune pathway and improving the efficacy of epithelial OC immunotherapy [57]. In high-grade serous OC, cGAS/STING-mediated activation of the restrictive aging-related secretory phenotype is sufficient to induce immune infiltration and sensitize the homologous recombination deficient high-grade serous OC to immune checkpoint blockade [58]. Additionally, the cGAS/STING pathway plays an important role in the disease by regulating pyroptosis. 4-octyl itaconate can ameliorate alveolar macrophage pyroptosis in acute respiratory distress syndrome by rescuing mitochondrial dysfunction and inhibiting the cGAS/STING pathway [59]. Activation of the cGAS-STING axis contributes to neuroinflammation and induces inflammasome activation and microglial pyroptosis in a mouse model of neuroinflammatory injury and cerebral venous sinus thrombosis [60]. In our research, knockdown of CENPM activated cGAS-STING pathway and the cGAS inhibitor reversed the inhibitory effect of CENPM knockdown on OC progression. Taken together, knockdown of CENPM inhibited OC progression via activating cGAS-STING pathway and promoting pyroptosis of OC cells. The cGAS/STING pathway is a promising target for the treatment of OC.

This research also has some limitations. For instance, due to the limited funding and insufficient experimental

period, we did not use two or more siRNAs to knock down CENPM to exclude off-target effects. This study also lacks relevant validations based on clinical samples due to the limitations of laboratory conditions and clinical samples. Additionally, the exploration of the role of chromosomal segregation defect caused by CENPM deficiency will contribute to improving our findings. We will improve the laboratory conditions and collect more clinical samples to refine our research in the future.

In conclusion, KIFC1, PCLAF, CDCA5, KNTC1, MCM3, OIP5, CENPM, KIF15, and ASF1B were identified as hub genes with high diagnostic value. CENPM, a key hub gene of OC, was overexpressed in OC, which was determined as a potential biomarker. Knockdown of CENPM promoted pyroptosis and inhibited the progression of OC via activating cGAS-STING pathway. Our findings indicate that CENPM may be a promising molecular target and a potential therapeutic for OC, which can provide a new insight into pathogenesis of OC and help us understand the underlying mechanism associated with OC.

Supplementary Information

The online version contains supplementary material available at <https://doi.org/10.1186/s12885-024-12296-5>.

Supplementary Material 1.

Supplementary Material 2.

Acknowledgements

Not applicable.

Authors' contributions

Wei Xie: Substantial contributions to conception and design, data acquisition, drafting the article; Leiyong Zhang, Junjing Shen and Fengdi Lai: data acquisition, drafting the article; Wenling Han and Xiaoyan Liu: data acquisition; reviewing the article; All the authors took part in the experiment. All the authors read and approved the manuscript.

Funding

Jiangxi Science, Technology and Health Commission Plan (No. 202310769).

Availability of data and materials

The datasets generated and/or analyzed during the current study are available in GEO of National Center for Biotechnology Information repository, [www.ncbi.nlm.nih.gov/geo/browse/?view=series]. The original analysis data, volcano graph, and data chart can be obtained from GEO2R repository, [www.ncbi.nlm.nih.gov/geo/geo2r]. The data of hub genes expression in tumor tissue and normal tissue can be downloaded from GEPIA2 repository, [<http://gepia2.cancer-pku.cn/#index>]. Primer sequences are available from National Center for Biotechnology Information repository, [<https://www.ncbi.nlm.nih.gov/>].

Declarations

Ethical approval and consent to participate

The animal experiments conformed to the Guide for the Care and Use of Laboratory Animals. Animal study has been approved by the Animal Ethics Committee of First Affiliated Hospital of Gannan Medical University.

All experiments were performed in accordance with relevant guidelines and regulations.

The manuscript reporting adheres to the ARRIVE guidelines for the reporting of animal experiments.

Consent for publication

Not applicable.

Competing interests

The authors declare no competing interests.

Received: 3 July 2023 Accepted: 22 April 2024

Published online: 01 May 2024

References

- Gong X, et al. Exosomes: a potential tool for immunotherapy of ovarian cancer. *Front Immunol*. 2022;13:1089410.
- Mei S, et al. Tumor microenvironment in ovarian cancer peritoneal metastasis. *Cancer Cell Int*. 2023;23(1):11.
- Varier L, et al. An overview of ovarian cancer: the role of cancer stem cells in chemoresistance and a precision medicine approach targeting the Wnt pathway with the antagonist sFRP4. *Cancers (Basel)*. 2023;15(4):1275.
- Bose S, et al. Chemokines driven ovarian cancer progression, metastasis and chemoresistance: potential pharmacological targets for cancer therapy. *Semin Cancer Biol*. 2022;86(Pt 2):568–79.
- Qin T, et al. Harnessing preclinical models for the interrogation of ovarian cancer. *J Exp Clin Cancer Res*. 2022;41(1):277.
- Bhardwaj V, et al. Neo-vascularization-based therapeutic perspectives in advanced ovarian cancer. *Biochim Biophys Acta Rev Cancer*. 2023;1878(3):188888.
- Huffman OG, et al. Mechanistic insights on hyperthermic intraperitoneal chemotherapy in ovarian cancer. *Cancers (Basel)*. 2023;15(5):1402.
- Jiang B, et al. The miR-1290/OGN axis in ovarian cancer-associated fibroblasts modulates cancer cell proliferation and invasion. *J Ovarian Res*. 2024;17(1):52.
- Nevins S, et al. Nanotechnology approaches for prevention and treatment of chemotherapy-induced neurotoxicity, neuropathy, and cardiomyopathy in breast and ovarian cancer survivors. *Small*. 2023:e2300744.
- Perpelescu M, Fukagawa T. The ABCs of CENPs. *Chromosoma*. 2011;120(5):425–46.
- Tanaka K, Hirota T. Chromosomal instability: a common feature and a therapeutic target of cancer. *Biochim Biophys Acta*. 2016;1866(1):64–75.
- Johnson SC, McClelland SE. Watching cancer cells evolve through chromosomal instability. *Nature*. 2019;570(7760):166–7.
- Xiao Y, et al. Upregulation of CENPM promotes hepatocarcinogenesis through multiple mechanisms. *J Exp Clin Cancer Res*. 2019;38(1):458.
- Wang X, et al. High expression of centromere protein N as novel biomarkers for gastric adenocarcinoma. *Cancer Rep (Hoboken)*. 2023;6(4):e1798.
- Wang J, et al. Centromere protein I (CENP-I) is upregulated in gastric cancer, predicts poor prognosis, and promotes tumor cell proliferation and migration. *Technol Cancer Res Treat*. 2021;20:15330338211045510.
- He P, et al. Reduced expression of CENP-E contributes to the development of hepatocellular carcinoma and is associated with adverse clinical features. *Biomed Pharmacother*. 2020;123:109795.
- Zhang Y, et al. HJURP inhibits proliferation of ovarian cancer cells by regulating CENP-A/CENP-N. *Bull Cancer*. 2022;109(10):1007–16.
- Lee YC, et al. Overexpression of centromere protein K (CENPK) in ovarian cancer is correlated with poor patient survival and associated with predictive and prognostic relevance. *PeerJ*. 2015;3:e1386.
- Zou Z, et al. The role of pyroptosis in hepatocellular carcinoma. *Cell Oncol (Dordr)*. 2023;46:811–23.
- Li M, et al. Photon-controlled pyroptosis activation (photopyro): an emerging trigger for antitumor immune response. *J Am Chem Soc*. 2023;145(11):6007–23.
- Ju X, et al. Role of pyroptosis in cancer cells and clinical applications. *Biochimie*. 2021;185:78–86.
- Wen J, et al. NLRP3 inflammasome-induced pyroptosis in digestive system tumors. *Front Immunol*. 2023;14:1074606.
- Yang C, et al. CBL0137 activates ROS/BAX signaling to promote caspase-3/GSDME-dependent pyroptosis in ovarian cancer cells. *Biomed Pharmacother*. 2023;161:114529.
- Sun J, et al. Exposure to Di-(2-Ethylhexyl) phthalate drives ovarian dysfunction by inducing granulosa cell pyroptosis via the SLC39A5/NF- κ B/NLRP3 axis. *Ecotoxicol Environ Saf*. 2023;252:114625.
- Huo J, et al. BI 2536 induces gasdermin E-dependent pyroptosis in ovarian cancer. *Front Oncol*. 2022;12:963928.
- Jiang M, et al. cGAS-STING, an important pathway in cancer immunotherapy. *J Hematol Oncol*. 2020;13(1):81.
- Burdette DL, Vance RE. STING and the innate immune response to nucleic acids in the cytosol. *Nat Immunol*. 2013;14(1):19–26.
- Dhanwani R, Takahashi M, Sharma S. Cytosolic sensing of immuno-stimulatory DNA, the enemy within. *Curr Opin Immunol*. 2018;50:82–7.
- Kwon J, Bakhoun SF. The cytosolic DNA-sensing cGAS-STING pathway in cancer. *Cancer Discov*. 2020;10(1):26–39.
- Berger G, Marloye M, Lawler SE. Pharmacological modulation of the STING pathway for cancer immunotherapy. *Trends Mol Med*. 2019;25(5):412–27.
- Sivick KE, et al. Magnitude of therapeutic STING activation determines CD8+ T cell-mediated anti-tumor immunity. *Cell Rep*. 2018;25(11):3074–3085.e5.
- Wu J, et al. Interferon-independent activities of mammalian STING mediate antiviral response and tumor immune evasion. *Immunity*. 2020;53(1):115–126.e5.
- Wu J, et al. STING-mediated disruption of calcium homeostasis chronically activates ER stress and primes T cell death. *J Exp Med*. 2019;216(4):867–83.
- Xiao Y, et al. Multi-omics approaches for biomarker discovery in early ovarian cancer diagnosis. *EBioMedicine*. 2022;79:104001.
- Buklaho PA, et al. Molecular features as promising biomarkers in ovarian cancer. *Adv Clin Exp Med*. 2023;32:1029–40.
- Chen J, et al. Non-apoptotic cell death in ovarian cancer: treatment, resistance and prognosis. *Biomed Pharmacother*. 2022;150:112929.
- Pilvenyte G, et al. Molecularly imprinted polymers for the determination of cancer biomarkers. *Int J Mol Sci*. 2023;24(4):4105.
- Li J, et al. Kinesin Family Member C1 (KIFC1) Regulated by Centrosome Protein E (CENPE) promotes proliferation, migration, and epithelial-mesenchymal transition of ovarian cancer. *Med Sci Monit*. 2020;26:e927869.
- Jia YS, et al. Beta-catenin knockdown impairs the viability of ovarian cancer cells by modulating YAP-dependent glycolysis. *Am J Transl Res*. 2023;15(2):982–94.
- Liu J, et al. Identification of potential biomarkers in association with progression and prognosis in epithelial ovarian cancer by integrated bioinformatics analysis. *Front Genet*. 2019;10:1031.
- Pan W, et al. KNTC1, regulated by HPV E7, inhibits cervical carcinogenesis partially through Smad2. *Exp Cell Res*. 2023;423(1):113458.
- Kang EY, et al. MCM3 is a novel proliferation marker associated with longer survival for patients with tubo-ovarian high-grade serous carcinoma. *Virchows Arch*. 2022;480(4):855–71.
- Zhang X, et al. The role of OIP5 in the carcinogenesis and progression of ovarian cancer. *J Ovarian Res*. 2023;16(1):185.
- Singh R, Som A. Common miRNAs, candidate genes and their interaction network across four subtypes of epithelial ovarian cancer. *Bioinformatics*. 2021;17(8):748–59.
- Shen J, et al. Identification of key biomarkers associated with development and prognosis in patients with ovarian carcinoma: evidence from bioinformatic analysis. *J Ovarian Res*. 2019;12(1):110.
- Huang L, et al. Identification of survival-associated hub genes in pancreatic adenocarcinoma based on WGCNA. *Front Genet*. 2021;12:814798.
- Liu X, Wang H, Zhao G. Centromere protein A goes far beyond the centromere in cancers. *Mol Cancer Res*. 2022;20(1):3–10.
- Liu C, et al. Upregulation of CENPM facilitates lung adenocarcinoma progression via PI3K/AKT/mTOR signaling pathway. *Acta Biochim Biophys Sin (Shanghai)*. 2022;54(1):99–112.
- Zheng C, et al. Upregulation of CENPM facilitates tumor metastasis via the mTOR/p70S6K signaling pathway in pancreatic cancer. *Oncol Rep*. 2020;44(3):1003–12.

50. Liu T, et al. Pyroptosis: a developing foreland of ovarian cancer treatment. *Front Oncol.* 2022;12:828303.
51. Ye Y, Dai Q, Qi H. A novel defined pyroptosis-related gene signature for predicting the prognosis of ovarian cancer. *Cell Death Discov.* 2021;7(1):71.
52. Li J, et al. LncRNA GAS5 suppresses ovarian cancer by inducing inflammasome formation. *Biosci Rep.* 2018;38(2):BSR20171150.
53. Tan C, et al. LncRNA HOTTIP inhibits cell pyroptosis by targeting miR-148a-3p/AKT2 axis in ovarian cancer. *Cell Biol Int.* 2021;45(7):1487–97.
54. Qiao L, et al. α -NETA induces pyroptosis of epithelial ovarian cancer cells through the GSDMD/caspase-4 pathway. *Faseb j.* 2019;33(11):12760–7.
55. de Queiroz N, et al. Ovarian cancer cells commonly exhibit defective STING signaling which affects sensitivity to viral oncolysis. *Mol Cancer Res.* 2019;17(4):974–86.
56. Yang D, et al. Loss of HRD functional phenotype impedes immunotherapy and can be reversed by HDAC inhibitor in ovarian cancer. *Int J Biol Sci.* 2023;19(6):1846–60.
57. Cornelison R, et al. CX-5461 treatment leads to cytosolic DNA-mediated STING activation in ovarian cancer. *Cancers (Basel).* 2021;13(20):5056.
58. Paffenholz SV, et al. Senescence induction dictates response to chemo- and immunotherapy in preclinical models of ovarian cancer. *Proc Natl Acad Sci U S A.* 2022;119(5):e2117754119.
59. Wu YT, et al. 4-octyl itaconate ameliorates alveolar macrophage pyroptosis against ARDS via rescuing mitochondrial dysfunction and suppressing the cGAS/STING pathway. *Int Immunopharmacol.* 2023;118:110104.
60. Ding R, et al. Activating cGAS-STING axis contributes to neuroinflammation in CVST mouse model and induces inflammasome activation and microglia pyroptosis. *J Neuroinflammation.* 2022;19(1):137.

Publisher's Note

Springer Nature remains neutral with regard to jurisdictional claims in published maps and institutional affiliations.